Int J Adv Struct Eng
DOI 10.1007/s40091-016-0111-3

ORIGINAL RESEARCH

Optimal placement of active braces by using PSO algorithm in near- and far-field earthquakes

M. Mastali[1] · A. Kheyroddin[2,3] · B. Samali[4] · R. Vahdani[2]

Received: 16 February 2015 / Accepted: 1 February 2016

Abstract One of the most important issues in tall buildings is lateral resistance of the load-bearing systems against applied loads such as earthquake, wind and blast. Dual systems comprising core wall systems (single or multi-cell core) and moment-resisting frames are used as resistance systems in tall buildings. In addition to adequate stiffness provided by the dual system, most tall buildings may have to rely on various control systems to reduce the level of unwanted motions stemming from severe dynamic loads. One of the main challenges to effectively control the motion of a structure is limitation in distributing the required control along the structure height optimally. In this paper, concrete shear walls are used as secondary resistance system at three different heights as well as actuators installed in the braces. The optimal actuator positions are found by using optimized PSO algorithm as well as arbitrarily. The control performance of buildings that are equipped and controlled using the PSO algorithm method placement is assessed and compared with arbitrary placement of controllers using both near- and far-field ground motions of Kobe and Chi–Chi earthquakes.

Keywords Pole assignment method · Near- and far-field earthquakes · PSO algorithm · Optimal actuator position

Introduction

The rapid growth of the urban population and consequent pressure on limited space have considerably influenced city residential development. The high cost of land, the desire to avoid ongoing urban sprawl, and the need to preserve important agricultural land have all contributed to drive residential buildings upward. Nowadays, high-rise buildings have become one of the impressive reflections and icons of today's civilization. The outlook of cities all over the world has been changing with these tall and slender structures (Smith and Coull 1991). Tall buildings use load-resisting systems against applied lateral loads such as concrete shear walls and core wall systems. The main problem of these systems is their limitations in controlling the response of super tall buildings (Kheyroddin et al. 2014; Keshavarz et al. 2011). Therefore, some strategies have been used to control and make serviceable tall buildings in addition to the lateral load-resisting systems which included: (1) passive control; (2) semi-active control; (3) active control, or their combinations. In the passive control, the structure uses its internal energy to dissipate external energy. A large number of studies have been conducted on the active control concept (Yang et al. 2004; Kwok et al. 2006). These systems are able to control the structure displacements, accelerations and internal forces by using external energy and providing a direct counteracting force by the actuators. Using this strategy for controlling structures against external excitation has limitations because of some technological and economic aspects (Symans and Constantinou 1999), as well as the

✉ M. Mastali
m.mastali@civil.uminho.pt; muhammad.mastali@gmail.com

[1] Department of Civil Engineering, ISISE, Minho University, Campus de Azurem, 4800-058 Guimaraes, Portugal

[2] Faculty of Civil Engineering, Semnan University, Seman, Iran

[3] Department of Civil Engineering and Applied Mechanics, University of Texas, Arlington, TX, USA

[4] School of Civil and Environmental Engineering, University of Western Sydney, Sydney, Australia

Published online: 15 February 2016

risks associated with loss of external power in the event of a major earthquake or severe wind load. These systems require high amount of external energy for controlling the structures in comparison with other strategies. Hence, to overcome this problem, semi-active control was proposed as a strategy which compensates for the shortcomings of active control. In this control method, structural properties such as damping and/or stiffness are altered by use of special devices with very little external energy to activate such systems. As a result, much lower amount of external energy is required to control the structures during external excitations and there is a potential in this method to achieve control levels similar to active systems (Amini and Vahdani 2008). Because of limitations in the number of actuators and due to economic reasons, actuator location is an important issue in control problems. Nowadays, numerical methods, such as those inspired by nature, are used in optimizing actuator locations. These methods include ant colony, genetic algorithm, PSO (particle swarm optimization) algorithm, etc.

In this paper, three 3D buildings with different heights are used to investigate the effectiveness of the designed controller. In these systems, the concrete shear walls were also considered as the secondary load-resisting system.

In the present study, three structures with 21, 15, and 9 stories were studied, considering 3, 2, and 1 actuator, respectively. The actuators were placed in the system in two ways, which include (1) finding the optimized position of the optimized actuator using the PSO algorithm; (2) installing an actuator at arbitrary positions. Structures were modelled in MATLAB software. In this regard, finite element method was used for modelling these structures and the interactions between the frame and walls (Ghali et al. 2003). The obtained stiffness from this method was used in modelling of structures in MATLAB software. The novelty of the present paper was using PSO algorithm to optimize actuator locations.

Analysis of a planar frame in the presence of shear walls

The contribution of shear walls in a frame depends on the wall stiffness with respect to other structural elements. Commonly, it is assumed that horizontal forces are applied at the floor levels. Moreover, it is assumed that floor stiffness in the horizontal direction is very high compared to the stiffness of columns and shear walls. Therefore, it is assumed that the floors move as rigid bodies in the horizontal direction. Let us consider the structure shown in Fig. 1, which is constructed of some parallel frames with symmetrical axes.

Some of these structures use shear walls as the secondary load-resisting system. Because of geometric and loading symmetry, floors move without any rotation. By assuming rigid body motion for the floors, each level has a displacement equal to $[D^*]$. The stiffness matrix $[S]_{\text{nxn}}$ (n is the number of stories) corresponding to the coordinate $\{D^*\}$ for each planar frame is calculated and then all the stiffness matrices are assembled to obtain the stiffness matrix of the structure:

$$[S^*] = \sum_{i=1}^{m} [S^*]_i, \tag{1}$$

where m is the number of frames. The lateral movement at the floor level is calculated using the following equation in which $\{F\}$ is the applied force vector on each floor level:

$$[S^*]_{n\times n}\{D^*\}_{n\times 1} = \{F^*\}_{n\times 1}. \tag{2}$$

Approximate analysis of the planar structures

The shear wall deformations are similar to cantilever beams. This simplification is reasonable due to the fact that the rotations are constrained at the ends of the columns by beams in tension (Ghali et al. 2003). It is obvious that shear wall moment of inertia, I, is higher than that of the beam which subsequently leads to reduction in the beam ability to control rotations caused by deformation of the cantilever beam at the floor level. The observed behaviour suggests that the load-resisting systems are composed of two parts; see Figs. 2 and 3.

They are composed of (1) shear wall system; (2) equivalent column. Moment of inertia (I_{W}) of the shear wall and the column (I_{C}) at each floor level is equal to the sum of moments of inertia of the shear walls and the columns at that floor level. The second system is an equivalent column which is connected to the beams in a rigid way. Additionally, it is obvious that these two load-resisting systems are connected to each other by non-deformable tension elements and that all the external forces are applied at the floor level. Axial deformations in all structural elements are neglected, while shear deformations in walls and columns can be considered or neglected in the analysis. In case the shear deformations are considered, the effective (reduced) area is equal to the sum of the reduced areas of the walls and the columns at each floor level. It is assumed that the idealized structure has n degrees of freedom, representing the lateral movements of the floors. The stiffness matrix of the structure $\left[S^*_{n\times n}\right]$ is obtained by summing the stiffness matrices of the two resisting systems:

$$[S^*] = [S^*]_{\text{w}} + [S^*]_{\text{r}}, \tag{3}$$

where $[S^*]_{\text{r}}$ and $[S^*]_{\text{W}}$ are the stiffness matrices of the resisting frame and the wall, respectively, corresponding to

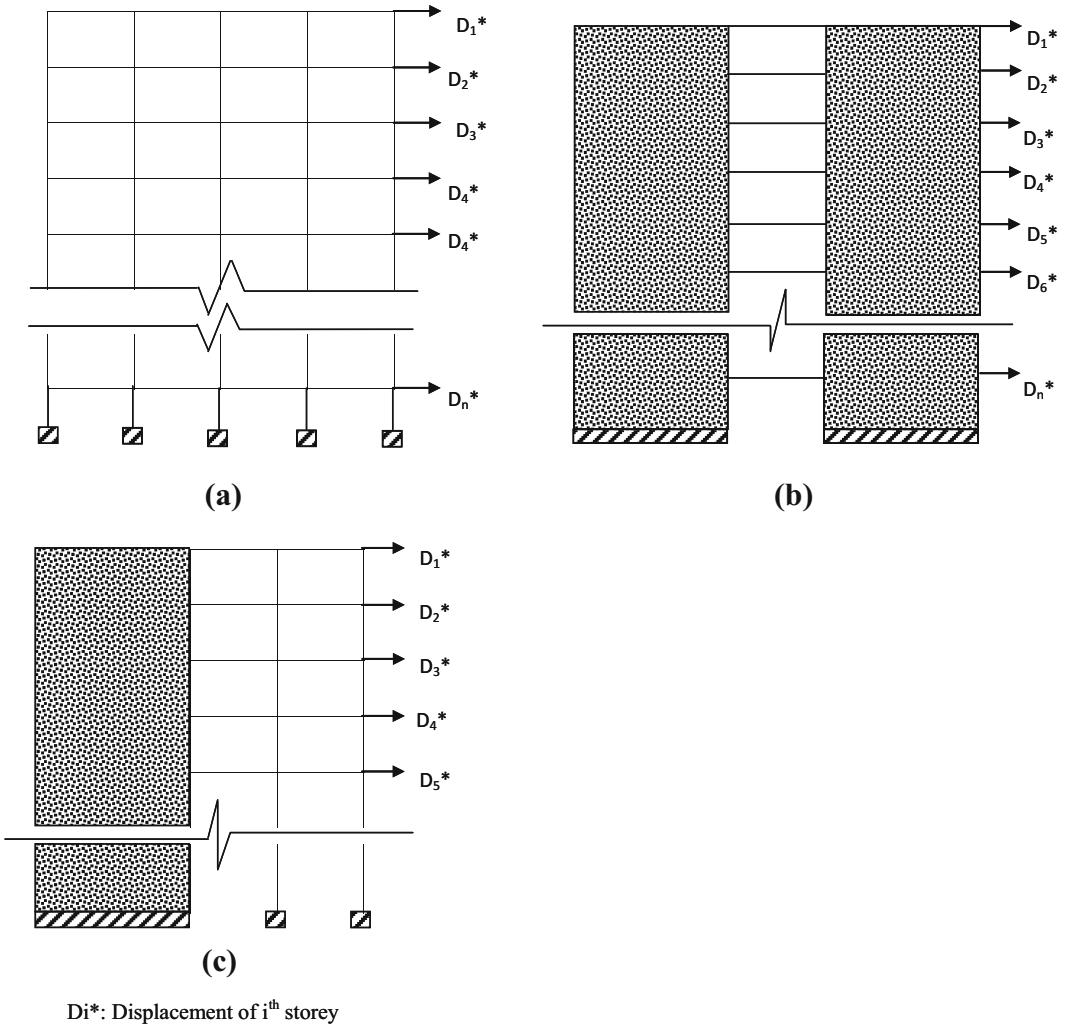

Fig. 1 Considered planar frames in the analysis of three dimension and geometrical symmetry: **a** concrete moment resistance frame; **b** symmetric concrete shear walls; **c** asymmetric concrete shear wall (Ghali et al. 2003)

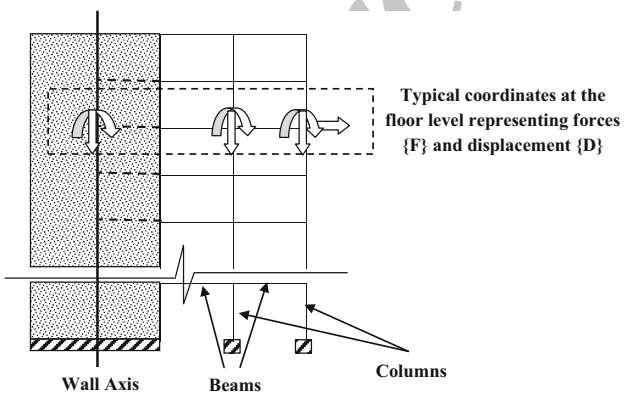

Fig. 2 Coordinate system corresponding to the stiffness matrix $[S]_i$ (Ghali et al. 2003)

n horizontal coordinates at floor levels. To determine $[S^*]_r$ and $[S^*]_W$ matrices, two degrees of freedom are considered at each floor level which consist of a rotation and a lateral movement for the wall and beam–column joint.

According to Fig. 3b, matrices $[S^*]_r$ and $[S^*]_w$ have $2n \times 2n$ degrees of freedom and then these two matrices, which relate the horizontal forces to the lateral movements with non-constrained rotations, are compacted. Therefore, the lateral movement at the floor level is obtained by solving the following equation:

$$[S^*]_{n\times n}\{D^*\}_{n+1} = \{F^*\}_{n\times 1}, \tag{4}$$

where $\{D^*\}$ represents the horizontal displacements of the shear walls or the columns at each floor level and $\{F^*\}$

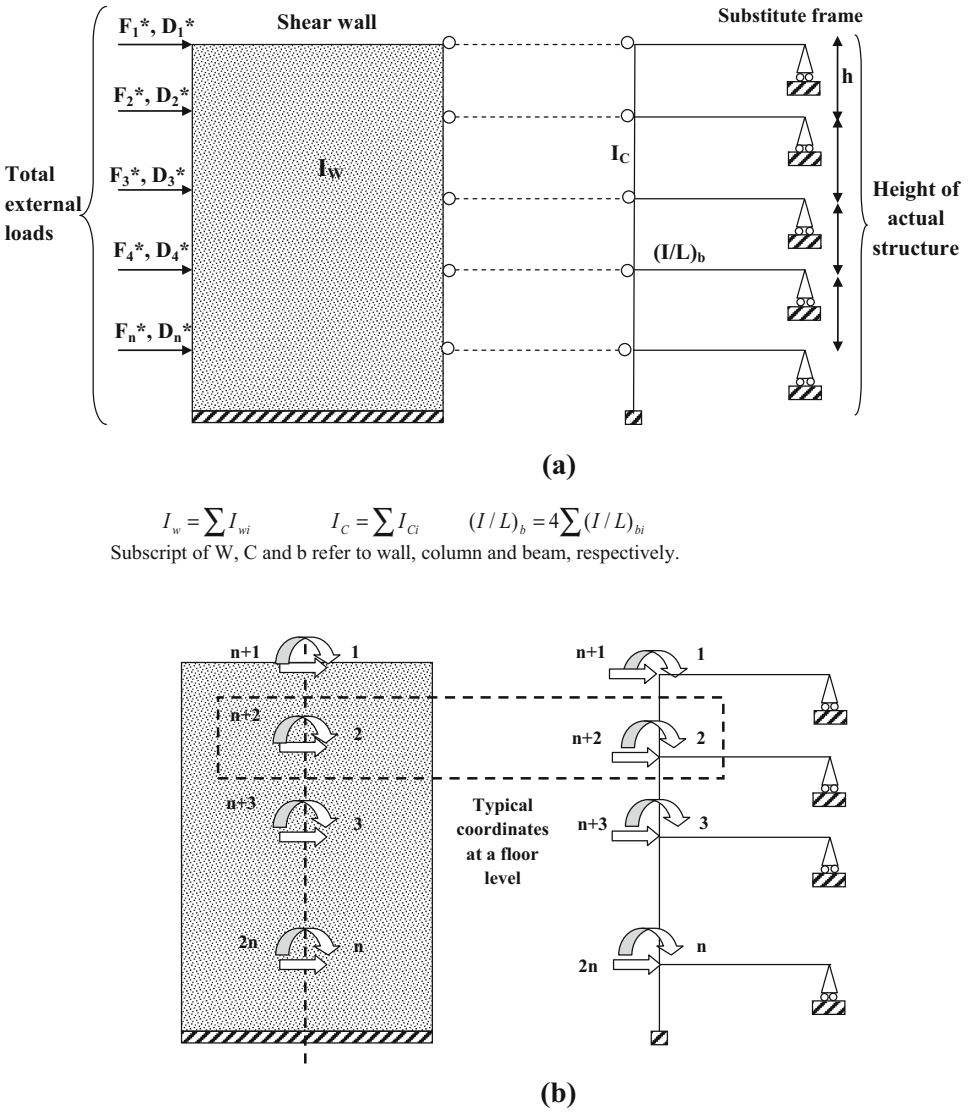

Fig. 3 Analysis of simplified structural frame: **a** idealized structure; **b** coordinates corresponding to stiffness matrices [S_r] and [S_w] (Ghali et al. 2003)

$$I_w = \sum I_{wi} \qquad I_C = \sum I_{Ci} \qquad (I/L)_b = 4\sum (I/L)_{bi}$$

Subscript of W, C and b refer to wall, column and beam, respectively.

represents the external loads which are imposed on the shear walls and the columns, i.e. $\{F^*\} = \{F^*\}_W + \{F^*\}_r$.

The applied forces to the shear wall and the frame can be calculated by:

$$\{F^*\}_w = [S^*]_w\{D^*\} \quad \{F^*\}_r = [S^*]_r\{D^*\}. \tag{5}$$

Then these forces are imposed on the shear wall and the frame and, subsequently, moments are determined at the end of the structural elements. If these moments are distributed in the structural elements such as shear walls and frames with regard of their corresponding flexural stiffnesses [(EI/h) or (EI/l)], then the approximate values of the actual end moments can be obtained. It is worth stating that if the shear walls are significantly different, or if there are great variations in the shear wall areas at each floor level, then the above calculation method can lead to false results. In this case, it is necessary to consider an idealized structure with more than one shear wall connected to the frame by means of tension elements, and the stiffness of each one must be calculated separately. Then the stiffness of the idealized structure can be calculated by summation of the distinct stiffnesses.

Special case: considering the same columns and beams

By considering the same cross-sectional areas for the columns and the beam elements, which leads to equal ratio of $(I/l)_b$ for all the stories, the frame matrix stiffness can be computed by the given equation:

$$[S]_{r_{2n\times 2n}} = \begin{bmatrix} [S_{11}]_r & [S_{12}]_r \\ [S_{21}]_r & [S_{22}]_r \end{bmatrix}, \tag{6}$$

in which the sub-matrices are:

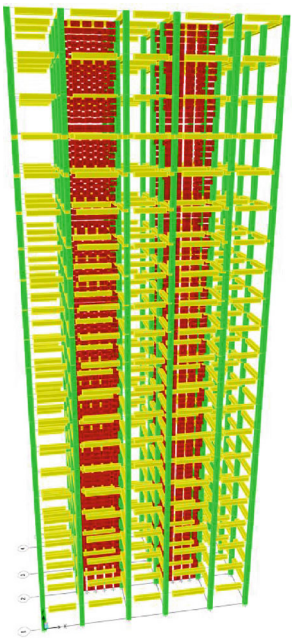

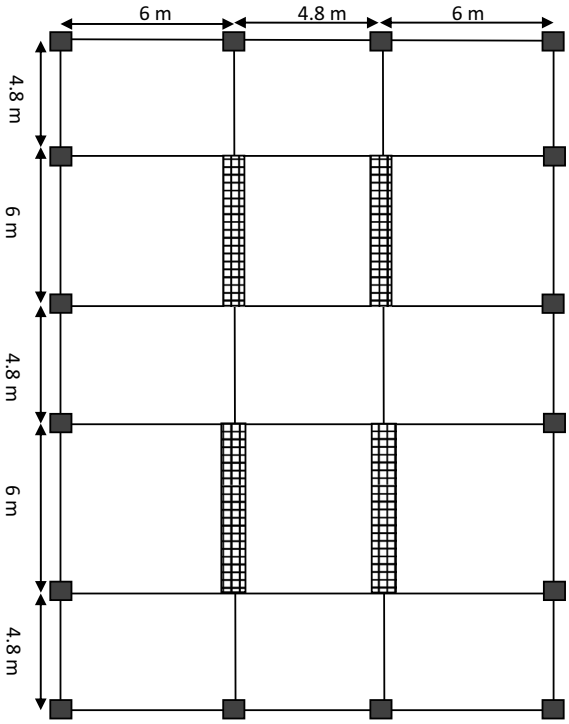

Fig. 4 Plan of structures and shear wall positions

$$[S_{11}]_{\mathrm{r}} = \frac{2(S+t)}{h^2}\begin{bmatrix} 1 & -1 & 0 & 0 & 0 & 0 & 0 & 0 \\ -1 & 2 & -1 & 0 & 0 & 0 & 0 & 0 \\ 0 & . & 2 & . & 0 & 0 & 0 & 0 \\ 0 & 0 & . & . & . & 0 & 0 & 0 \\ 0 & 0 & 0 & . & . & . & 0 & 0 \\ 0 & 0 & 0 & 0 & . & 2 & -1 & 0 \\ 0 & 0 & 0 & 0 & 0 & -1 & 2 & -1 \\ 0 & 0 & 0 & 0 & 0 & 0 & -1 & 2 \end{bmatrix}_{n\times n}, \tag{7}$$

$$[S_{21}]_{\mathrm{r}} = [S_{12}]_{\mathrm{r}}^{\mathrm{T}} = \frac{(S+t)}{h}\begin{bmatrix} -1 & 1 & 0 & 0 & 0 & 0 & 0 & 0 \\ -1 & 0 & 1 & 0 & 0 & 0 & 0 & 0 \\ 0 & -1 & 0 & 1 & 0 & 0 & 0 & 0 \\ 0 & 0 & . & . & . & 0 & 0 & 0 \\ 0 & 0 & 0 & . & . & . & 0 & 0 \\ 0 & 0 & 0 & 0 & . & . & . & 0 \\ 0 & 0 & 0 & 0 & 0 & -1 & 0 & 1 \\ 0 & 0 & 0 & 0 & 0 & 0 & -1 & 0 \end{bmatrix}_{n\times n}, \tag{8}$$

$$[S_{22}]_{\mathrm{r}} = S\begin{bmatrix} (1+\beta) & c & 0 & 0 & 0 & 0 & 0 & 0 \\ c & (2+\beta) & c & 0 & 0 & 0 & 0 & 0 \\ 0 & c & (2+\beta) & c & 0 & 0 & 0 & 0 \\ 0 & 0 & c & . & . & 0 & 0 & 0 \\ 0 & 0 & 0 & . & . & . & 0 & 0 \\ 0 & 0 & 0 & 0 & . & . & . & 0 \\ 0 & 0 & 0 & 0 & 0 & c & (2+\beta) & c \\ 0 & 0 & 0 & 0 & 0 & 0 & c & (2+\beta) \end{bmatrix}_{n\times n}, \tag{9}$$

where:

$$\beta = \frac{3E}{S}\left(I/L\right)_{\mathrm{b}} \quad S = \frac{(4+\alpha)}{(1+\alpha)}\frac{\mathrm{EI_c}}{h} \quad t = \frac{(2-\alpha)}{(1+\alpha)}\frac{\mathrm{EI_c}}{h} \quad c = \pi(t/S), \tag{10}$$

In which S is the rotational stiffness of a column when the support is clamped; t is the transferred moment and c is the transferred coefficient. The shear deformation of the vertical elements can be calculated by:

$$\alpha = \frac{12\mathrm{EI_c}}{h^2 G a_{\mathrm{rc}}} \tag{11}$$

and the shear deformation of the beams are neglected. The effective cross-sectional area of the columns is computed by adding all the effective cross-sectional areas of the columns ($a_{\mathrm{rc}} = \sum a_{\mathrm{rci}}$).

Modelling and specifications of the models

In this study, three 3D structures with 9, 15 and 21 stories are modelled. The plan of the structures and the shear wall positions are shown in Fig. 4. Moreover, the considered properties for the models are given in Table 1. Since the concrete shear walls were located in one direction and actuators will be placed in the same direction as the concrete shear walls as in Fig. 4, the simplified planar formulas in "Analysis of a planar frame in the presence of shear walls" could be used for modelling the interaction of frame and shear walls in the modelled three-dimensional structures.

Table 1 Considered properties of structures

	Shear wall	Frame	
a_{rw}	6.66	6.66	Considered equal for all structures
α	12.9	0	
β	0	17.8	
E	$10^7 \times 2236$ (N/m^2)	$10^7 \times 2236$ (N/m^2)	
υ	0.17	0.17	
G	$\left(\frac{1}{2.3}\right)E$	$\left(\frac{1}{2.3}\right)E$	
I_c	28.188 (m^4)	0.022 (m^4)	Considered for structures with 21 stories
$\left(\frac{I}{l}\right)_b$	0.25	0.25	
I_c	28.188 (m^4)	0.02 (m^4)	Considered for structures with 21 stories
$\left(\frac{I}{l}\right)_b$	0.22	0.22	
I_c	28.188 (m^4)	0.017 (m^4)	Considered for structures with 21 stories
$\left(\frac{I}{l}\right)_b$	0.20	0.20	

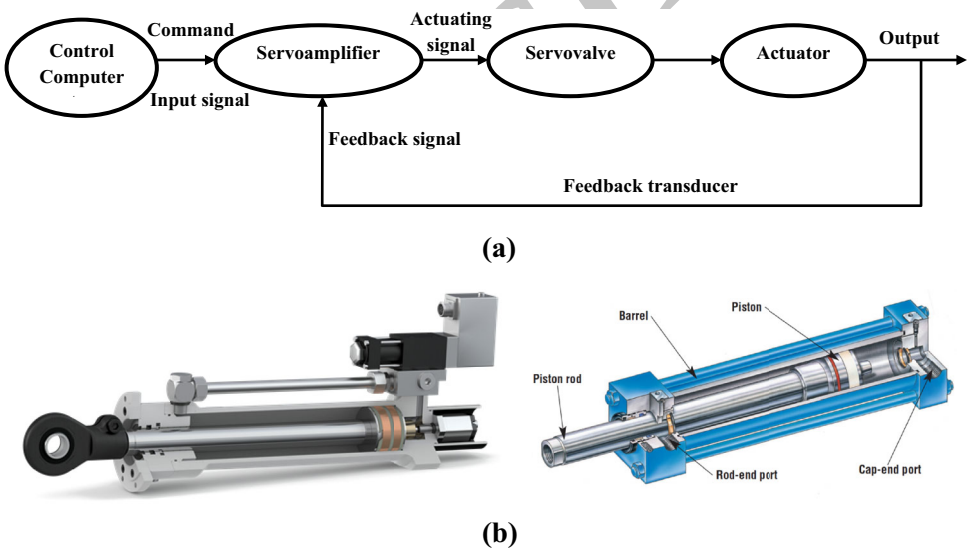

Fig. 5 **a** Servo-control electrohydraulic diagram; **b** schematic of a servo-hydraulic actuator (http://www.besmaklab.com/Products/133/Single-Ended_Servo_Hydraulic_Actuators/9)

All structures are modelled with the floor thicknesses and storey heights of 0.3 (m) and 3.3 (m), respectively. Actuators were used in the braces to control the structures. Using active brace control is one of the prominent strategies in control problems. This system is composed of pre-stressed systems or braces connected to the structure which are controlled by means of an electrohydraulic servocontrol system as shown in Fig. 5a. Moreover, a schematic view of a servo-hydraulic actuator is presented in Fig. 5b.

The hypotheses considered in the analysis and modelling are:

1. Damping for all the models are considered as 3 % of the critical.
2. To prevent saturation in the actuator, a constraint was defined as:

$$0.1 < \eta + \mu < 0.46, \tag{12}$$

where η and μ are the available values in the α and β matrices which are used to obtain the gain matrix. Saturation occurs in the actuators whenever the actuators work with their maximum capacity and, therefore, become unable to tolerate other loads. The main reason for using different heights for buildings is to investigate height effects on the actuator positions by considering near- and far-field earthquakes.

3. To calculate the floor weights, the Iranian national loading code was used.

Table 2 Nominated models

Name	Storey number	No of actuators	Method used for placement of actuators
M21-3-P	21	3	Optimization by using the PSO algorithm
M15-2-P	15	2	Optimization by using the PSO algorithm
M9-1-P	9	1	Optimization by using the PSO algorithm
M21-3-A	21	3	Arbitrary
M15-2-A	15	2	Arbitrary
M9-1-A	9	1	Arbitrary

The Chi–Chi and Kobe records as both near- and far-field ground motions were used to analyse models listed in Table 2 (http://peer.berkeley.edu/products/strong_ground_motion_db.html).

Properties of near- and far-field earthquakes

Obviously, there are some differences in the properties of near- and far-field earthquakes. Therefore, it seems necessary to investigate the effects of these differences on the buildings and to classify these effects. A distance shorter than 15 km from a fault line is referred to as near-fault zone; otherwise, it is known as far-field zone. In the near-field zone, earthquake effects depend on three main factors, namely (1) rupture mechanism; (2) rupture propagation directions with respect to the site, and (3) permanent displacement due to fault slippage. These factors create two phenomena, which are rupture directivity and step fling. Rupture directivity is also divided into two phenomena, which are forward directivity and backward directivity. Forward directivity effects lead to horizontal oscillations in the direction perpendicular to the fault line in the form of a horizontal pulse, which has much more significant effects on the structures in comparison with a parallel pulse to the fault line. These pulses lead to an increase in the nonlinear deformation demands of the structures. Near-fault ground motions have short duration with high amplitude and high to medium oscillation periods (International Institute of Earthquake Engineering and Seismology 2007; Alavi 2001; Galal and Ghobarah 2006; Stewart et al. 2001). The recorded databases of Kobe and Chi–Chi earthquakes were used to analyse the structures. Regard of FEMA 356, the geotechnical specifications should be taken into account in selection process of the earthquake record databases (Federal Emergency Management Agency 2000). Therefore, the frequency contents, spectrum, effective duration, and type of soil could be varied regard of construction site (Federal Emergency Management Agency 2000).

Pole Assignment controller design

In this study, Pole Assignment was used as the control method. The equation of motion of a multi-degree-of-freedom (MDOF) system by considering a force control under the effect of a specific excitation is:

$$[M]\ddot{X} + [C]\dot{X} + [K]\{X\} = -[M]\{\mathrm{I}\}\ddot{X}_{\mathrm{g}} - \{U_{\mathrm{C}}\}, \tag{13}$$

where $\{Uc\}$ is the control force vector which has a dimension equal to that of the displacement vector $(n \times 1)$. The negative sign on the right hand side of Eq. (13) shows that the applied force control is in the same direction with the formed internal resistance due to damping and stiffness of the structure. $[M]$, $[C]$ and $[K]$ are the mass, damping and stiffness matrices, respectively, and have the dimensions of $(n \times n)$. In Eq. (13), $\{I\}$ is the unit vector with the dimension of $(n \times 1)$ and x_{g} is the earthquake acceleration record. By transforming the equation of motion into state-space, Eq. (13) can be rewritten in the following form:

$$\{\dot{q}\} = [A]\{q\} + [Be]\ddot{x}_{\mathrm{g}} + [B_{\mathrm{U}}]\{u_{\mathrm{c}}\}, \tag{14}$$

where $[A]$ is the system matrix, $[B_{\mathrm{u}}]$ the actuator position matrix, [Be] the vector of external excitation position and $\{q\}$ the space vector. These matrices and vectors are given by:

$$[B_{\mathrm{U}}] = \begin{bmatrix} 0 \\ -M^{-1} \end{bmatrix} \quad [Be] = \begin{Bmatrix} 0 \\ -I \end{Bmatrix}, \qquad q = \begin{Bmatrix} x \\ \dot{x} \end{Bmatrix} \quad [A] = \begin{bmatrix} 0 & I \\ -M^{-1}K & -M^{-1}C \end{bmatrix}. \tag{15}$$

The force control U_{c} is obtained by multiplying the gain matrix in the space vector:

$$\{U_{\mathrm{C}}\} = [F]\{\,q\,\}. \tag{16}$$

The gain matrix is replaced by:

$$F = [F_{\mathrm{K}}, F_{\mathrm{C}}], \tag{17}$$

where F_{k} and F_{C} are the stiffness and damping type of matrices with dimensions of $(n \times n)$. These components can be obtained by the following equations:

$$[F_C] = [\alpha][C] \quad [F_K] = [\beta][K'], \tag{18}$$

in which $[\alpha]$ and $[\beta]$ are diagonal matrices defined by the following matrices:

$$[\alpha] = \begin{bmatrix} \alpha_1 & 0 & 0 & 0 & 0 \\ 0 & \alpha_2 & 0 & 0 & 0 \\ 0 & 0 & . & 0 & 0 \\ 0 & 0 & 0 & . & 0 \\ 0 & 0 & 0 & 0 & \alpha_n \end{bmatrix}$$
$$[\beta] = \begin{bmatrix} \beta_1 & 0 & 0 & 0 & 0 \\ 0 & \beta_2 & 0 & 0 & 0 \\ 0 & 0 & . & 0 & 0 \\ 0 & 0 & 0 & . & 0 \\ 0 & 0 & 0 & 0 & \beta_n \end{bmatrix}. \tag{19}$$

The stiffness and damping matrices are obtained from the stiffness and damping properties:

$$[k'] = \begin{bmatrix} k_1 & 0 & 0 & 0 & 0 \\ 0 & k_2 & 0 & 0 & 0 \\ 0 & 0 & . & 0 & 0 \\ 0 & 0 & 0 & . & 0 \\ 0 & 0 & 0 & 0 & k_n \end{bmatrix} \qquad C_i = 2\xi\omega_i M_i$$
$$M_i = \{\Phi_i^{\mathrm{T}}\}[m]\{\Phi_i\}, \tag{20}$$

where $\{\varphi_i\}$ and ω_i are related to the mode and frequency of the ith structure, respectively. By substituting Eq. (16) into Eq. (14), the following equation will be obtained:

$$\{\dot{q}\} = ([A] + [Bu][F])\{q\} + \{Be\}\ddot{x}_g. \tag{21}$$

The new system matrix is defined as:

$$[A_{con}] = [A] + [Bu][F]. \tag{22}$$

Substituting Eq. (22) into Eq. (21) leads to the following equation:

$$\{\dot{q}\} = [A_{con}]\{q\} + \{Be\}\ddot{x}_g. \tag{23}$$

In this paper, by means of particle swarm optimization (PSO) algorithm, the optimum values of $[\alpha]$ and $[\beta]$ matrices are calculated in such a way that the obtained gain matrix modifies the system to satisfy the objective function. By performing this process, the best actuator placements are defined to control the structure in the direction of objective function. In this study, the objective function is defined as:

$$Z = 0.1Z_1 + 0.45Z_2 + 0.45Z_3, \tag{24}$$

where the components Z_1, Z_2 and Z_3 are defined as:

$$Z_3 = \min \frac{\text{Max. Controlled Force}}{\text{Max. uncontrolled Force}},$$
$$Z_2 = \min \frac{\text{Max. Controlled Drift}}{\text{Max. Uncontrolled Drift}},$$
$$Z_1 = \min \frac{\text{Max. Controlled Dis.}}{\text{Max. uncontrolled Dis.}}.$$

Using multi-objective functions lead to the optimum placement, capacity and number of actuators in comparison with the time a single objective function is used. Using energy terms in the multi-objective functions leads to improvement in the control process of structures.

Particle swarm optimization (PSO) algorithm

Particle swarm optimization algorithm is used for optimizing difficult numerical functions and, based on the metaphor of human social interaction, is capable of mimicking the ability of human societies to process knowledge (Shayeghi et al. 2009). This algorithm has roots in two main component methodologies: (1) artificial life (such as bird flocking, fish schooling and swarming); (2) evolutionary computation (Kenedy and Eberhart 1995). The main issue in this algorithm is that potential solutions are flown through hyperspace and are accelerated towards better or more optimum solutions. Particles adjust their flights based on the flying experiences of themselves and their companions. It keeps the rout of its coordinates in hyperspace which is associated with its previous best fit solution and its peer corresponding to the overall best value acquired thus far by any other particles in the population. Vectors are taken as particle presentations, since most optimization problems are convenient for such variable presentations (Shayeghi et al. 2009). Actually, the fundamental principles behind swarm intelligence are adaptability, diverse response, proximity, quality and stability. It is adaptive, based on the change of the best group value. The response assignments between the individual and group values ensure a diversity of responses. The higher-dimensional space calculations of the PSO concept are needed to be done over a series of time steps (Shayeghi et al. 2009). The population is defined as the quality factors of the previous best individual values and the previous best group values. The principle of stability and state in the PSO algorithm are functioned to the population changes and the best group value changes, respectively (Kennedy et al. 2001; Clerc and Kennedy 2002). According to (Shayeghi et al. 2008), the optimization technique can be used to solve similar problems as the GA algorithm, and not involved with the difficulties of GA problems (Shayeghi

et al. 2008). By observing the obtained results from the analysed problems solved by the PSO algorithm, it was found that it was robust in solving problems featuring nonlinearity, non-differentiability and high dimensionality. The PSO algorithm is the search method to improve the speed of convergence and find the global optimum value of the fitness function (Shayeghi et al. 2009).

PSO begins with a population of random solutions "particles" in a D-dimension space. The *i*th particle is represented by Xi = (xi1, xi2,…,xiD) (Shayeghi et al. 2009). Each particle keeps the rout coordinates in hyper-space, associated with the fittest solution. The value of the fitness for particle *i*th (pbest) is also stored as Pi = (pi1, pi2,…,piD). The PSO algorithm keeps rout to approach the overall best value (gbest), and its location, obtained thus far by any particle in the population. The PSO algorithm consists of a step, involving changing the velocity of each particle towards its pbest and gbest according to Eq. (25).

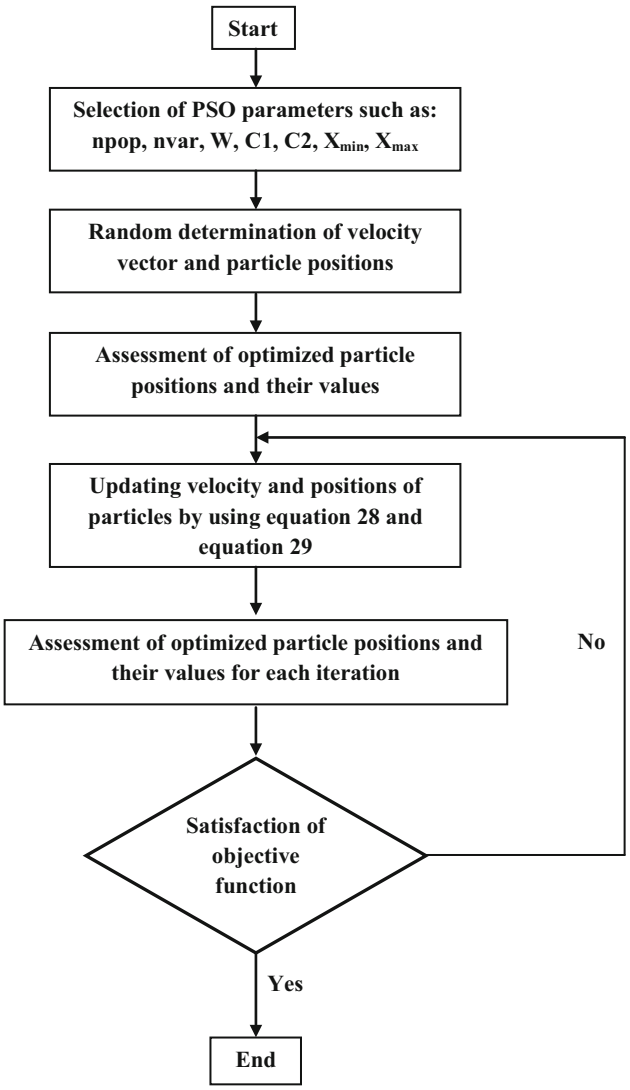

Fig. 6 Flowchart of the PSO algorithm

The velocity of particle *i* is represented as Vi = (vi1, vi2… viD). Acceleration is weighted by a random term, with separate random numbers being generated for acceleration towards pbest and gbest values. Then, the ith particle position is updated based on Eq. 26 (Kennedy et al. 2001):

$$v_i(t) = \phi\ v_i(t-1) + r_1 c_1(\vec{x}_{pbest} - \vec{x}_i) + r_2 c_2(\vec{x}_{gbest} - \vec{x}_i), \tag{25}$$

$$\vec{x}_i(t) = \vec{x}_i(t-1) + \vec{v}_i(t), \tag{26}$$

where C_1 and C_2 are acceleration coefficients. Kenedy showed that to ensure a stabilized solution, the sum of these coefficients must be less than 4; otherwise, velocity and particle positions tend to infinity (Clerc and Kennedy 2002). ϕ represents the inertia weights for which the following equation must be satisfied:

$$\phi \rangle 0.5(C_1 + C_2) - 1. \tag{27}$$

A flowchart is presented in Fig. 6 which better illustrates the mechanism of this algorithm.

Analytical results

Discussions

According to near- and far-field records of Kobe and Chi–Chi earthquakes (Fig. 7), structures with 9, 15 and 21 stories were analysed in MATLAB software. The positions of the actuators and the objective-function values are listed in Tables 3, 4, 5 and 6.

To assess the accuracy and sensitivity of the results, two records were used for analysing the structures. Chi–Chi earthquake has a long duration which can have different effects on the structures with different frequencies compared to Kobe earthquake that has a short duration.

For the structures with 21 stories, three actuators were installed on the top, middle and first floors regardless of the type of the external excitation zone. According to the obtained results shown in Fig. 8, for the tall building (21 stories), 67 % of the actuators are placed at the upper half of the structure and others are placed at the lower half. Moreover, for medium-rise structures (15 stories), 75 % of the actuators are placed at the upper half of the structure, while the others are installed on the ground floors. Finally, for the short building, the actuator position was dependent on the type of the external excitation zone. As seen in Fig. 8, structures having 21, 15, and 9 stories have 1, 0.71 and 0.42 height ratios, respectively.

As indicated in Fig. 9, the maximum displacement of the controlled and uncontrolled cases at the floor level throughout the structure height highlights the effect of adopted strategy for controlling the structures.

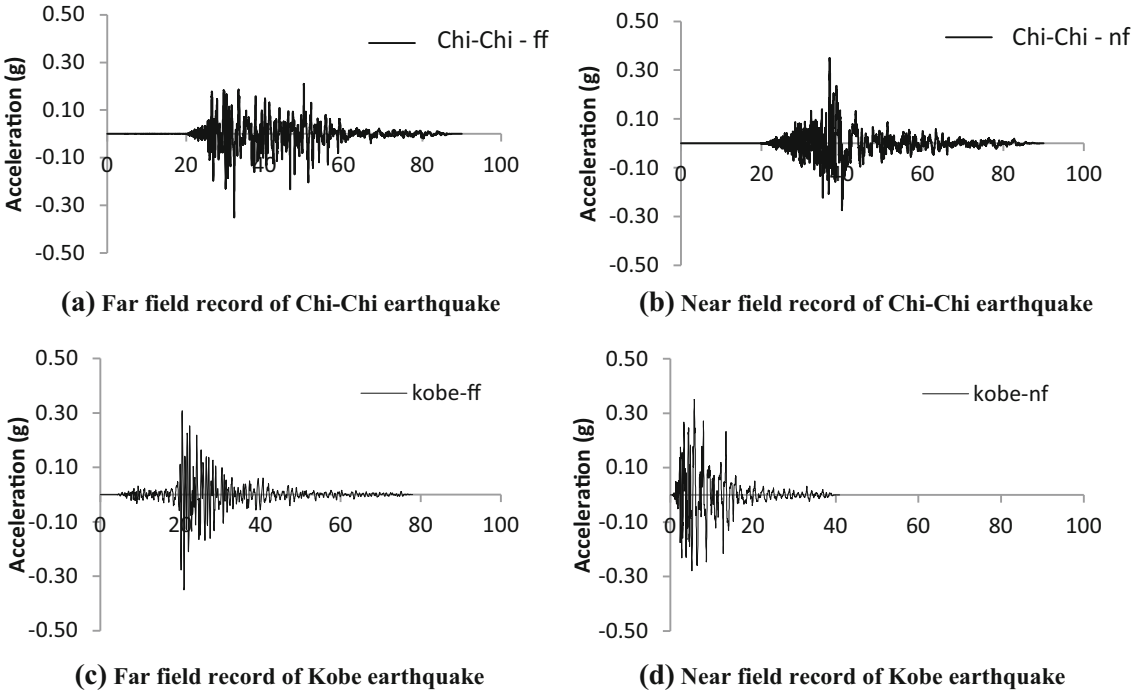

Fig. 7 Records of Chi–Chi and Kobe earthquake in both near and far field

Table 3 Actuator position and objective-function value for Kobe earthquake in the near field

Model	Actuator position	α	β	Objective function value (Z)
M21-3-P	1&16&18	0.25	0.2	0.1218
M15-2-P	9&13	0.25	0.2	0.1451
M9-1-P	7	0.25	0.2	0.2085
M21-3-A	7&14&21	0.2	0.25	0.1488
M15-2-A	7&15	0.2	0.25	0.1911
M9-1-A	6	0.2	0.25	0.2304

Table 4 Actuator position and objective-function value for Kobe earthquake in the far field

Model	Actuator position	α	β	Objective-function value (Z)
M21-3-P	1&16&18	0.25	0.2	0.1123
M15-2-P	1&13	0.25	0.2	0.2263
M9-1-P	8	0.25	0.2	0.2024
M21-3-A	7&14&21	0.2	0.25	0.1252
M15-2-A	7&15	0.2	0.25	0.2468
M9-1-A	6	0.2	0.25	0.2415

Table 5 Actuator position and objective-function value for Chi–Chi earthquake in the near field

Model	Actuator position	α	β	Objective-function value (Z)
M21-3-P	1&20&21	0.25	0.2	0.1101
M15-2-P	1&13	0.25	0.2	0.1804
M9-1-P	5	0.25	0.2	0.3187
M21-3-A	7&14&21	0.2	0.25	0.1257
M15-2-A	7&15	0.2	0.25	0.2043
M9-1-A	6	0.2	0.25	0.315

Table 6 Actuator position and objective-function value for Chi–Chi earthquake in the far field

Model	Actuator position	α	β	Objective-function value (Z)
M21-3-P	2&16&18	0.25	0.2	0.1158
M15-2-P	9&13	0.25	0.2	0.138
M9-1-P	9	0.25	0.2	0.2053
M21-3-A	7&14&21	0.2	0.25	0.1344
M15-2-A	7&15	0.2	0.25	0.1825
M9-1-A	6	0.2	0.25	0.2489

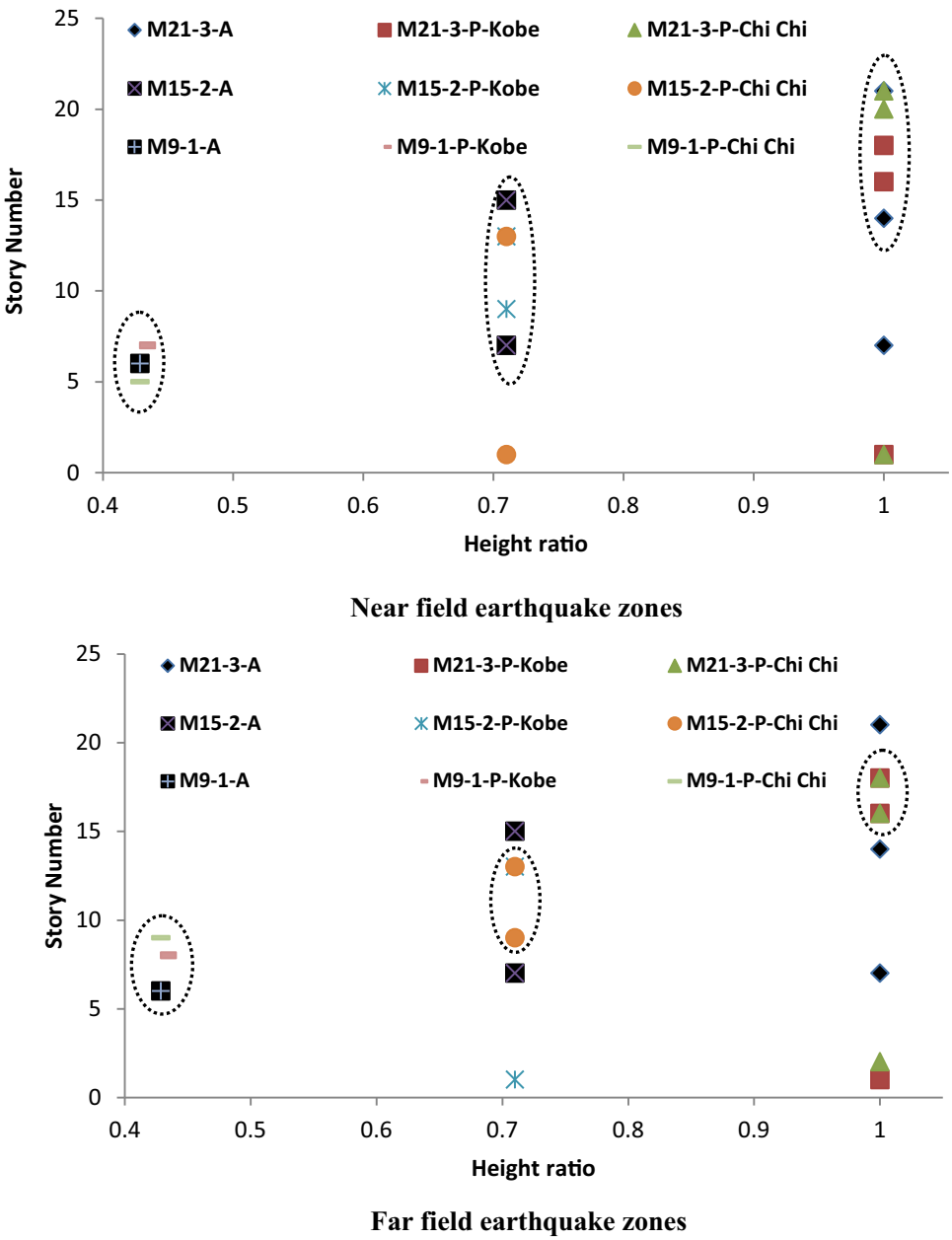

Fig. 8 Comparing actuator positions in near- and far-field zones by changing the height ratio

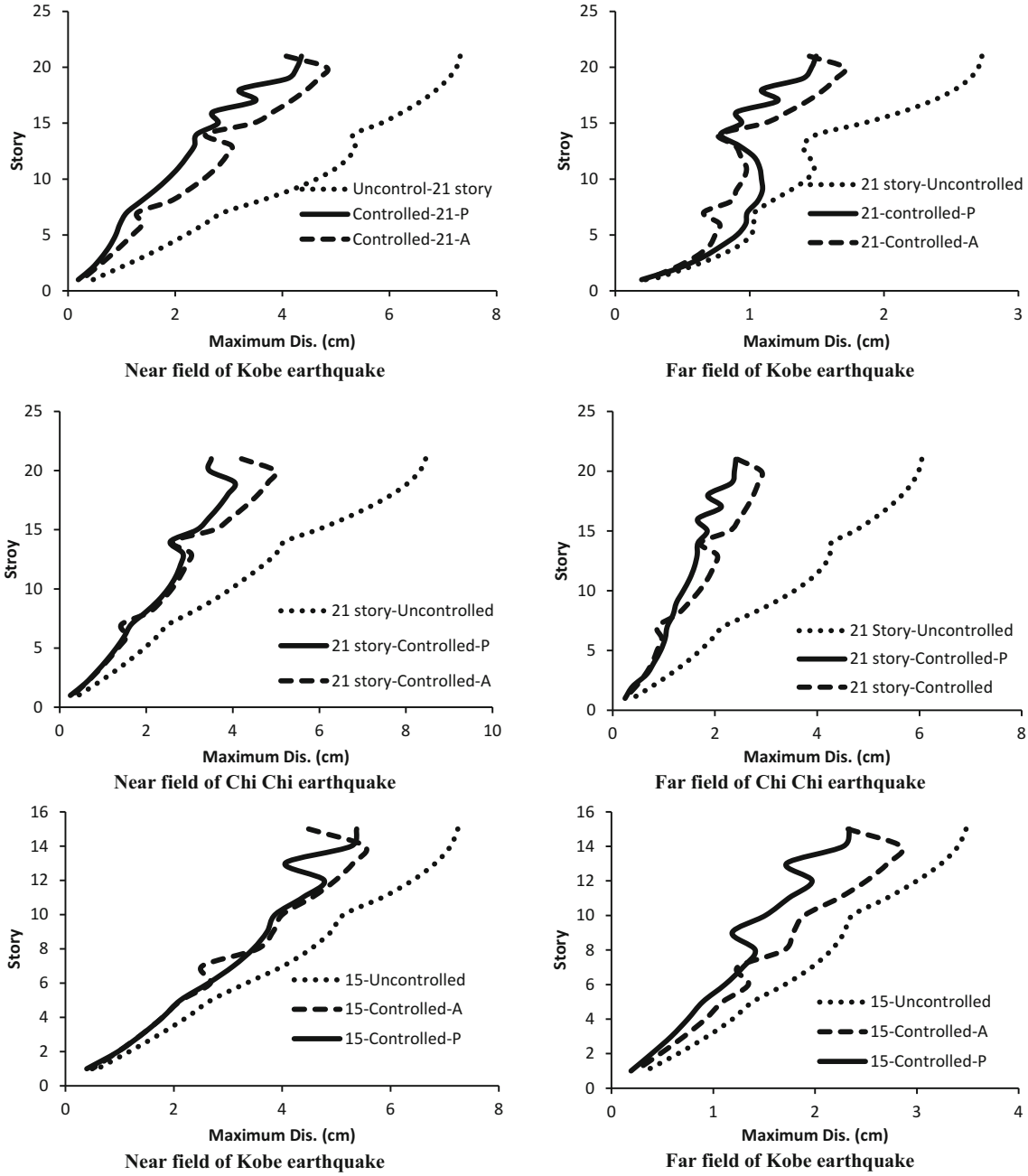

Fig. 9 Maximum controlled and uncontrolled displacements of structures throughout the height

Performance criteria

Some performance criteria introduced by Yang were used in this study to evaluate the controllers (Yang et al. 2004). The first criterion is related to the ability of the controller to reduce the maximum floor root mean square (RMS) acceleration:

$$J_1 = \max(\sigma_{\ddot{x}n})/\sigma_{\ddot{x}l}, \tag{28}$$

where $\sigma_{\ddot{x}_n}$ is the RMS acceleration of the storey in which the actuator is installed. $\sigma_{\ddot{x}_l}$ is the uncontrolled RMS acceleration of the top storey which does not have any controller or actuator. The second criterion is the average reduction in the acceleration of the controlled floors:

$$J_2 = \frac{1}{n}\sum \frac{\sigma_{\ddot{x}_i}}{\sigma_{\ddot{x}_0}}, \tag{29}$$

where n is number of floors in which the actuators were installed. $\sigma_{\ddot{x}_i}$ and $\sigma_{\ddot{x}_0}$ represent RMS acceleration in controlled and uncontrolled stories, respectively. The third and fourth criteria are used for evaluating the top floor displacements:

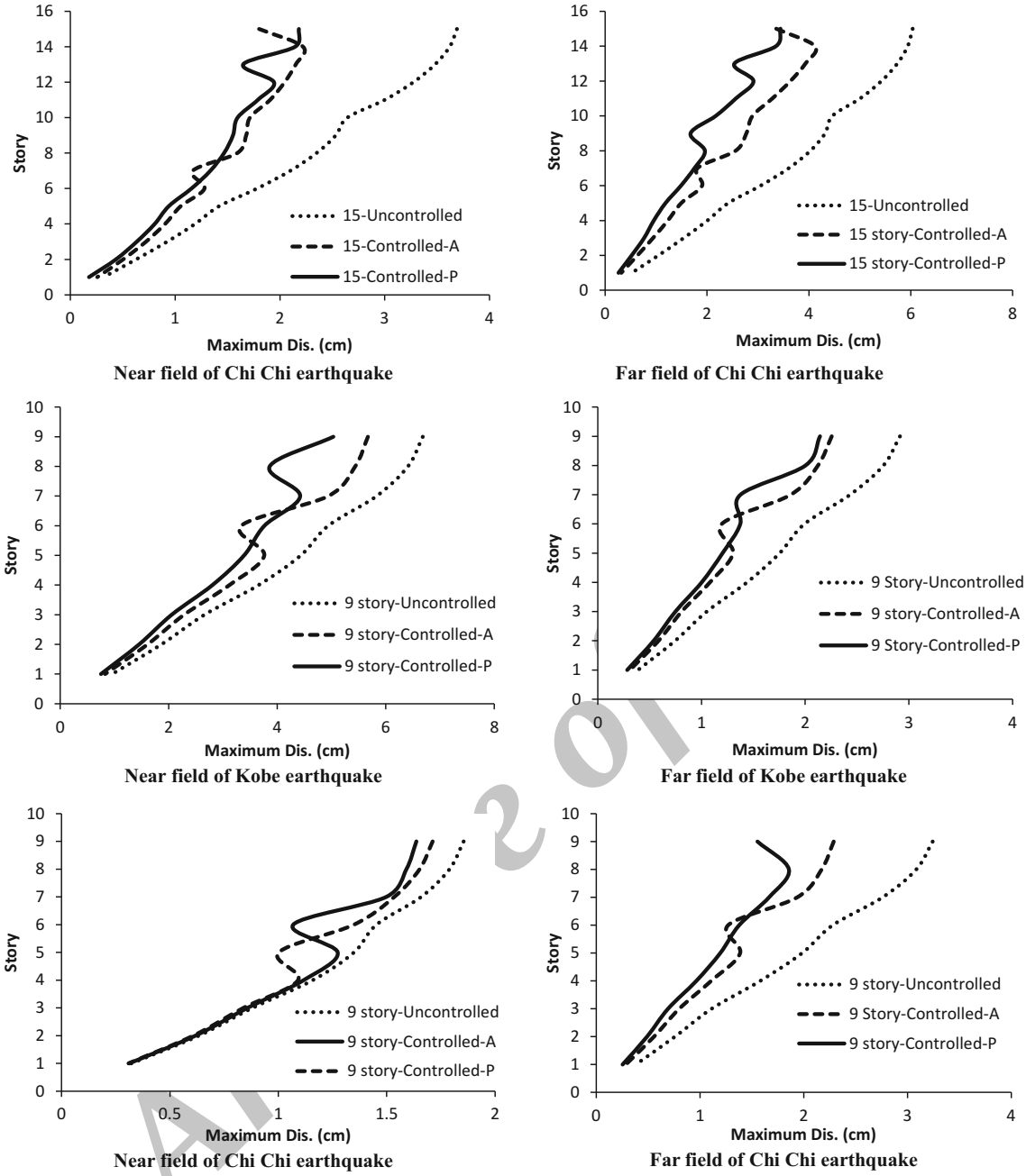

Fig. 9 continued

$$J_3 = \frac{\sigma_{x_l}}{\sigma_{x_0}}, \tag{30}$$

$$J_4 = \frac{1}{n}\sum \frac{\sigma_{x_i}}{\sigma_{x0}}, \tag{31}$$

where σ_{x_i} and σ_{x_0} are the uncontrolled and controlled RMS displacements at the top floor level, respectively. Furthermore, $\sigma_{\ddot{x}_i}$ and $\sigma_{\ddot{x}_0}$ represent the controlled and uncontrolled RMS accelerations in the storey, respectively. Three other criteria are used to assess the peak responses of the structure:

$$J_5 = \frac{\mathrm{Max}(\ddot{x}_i)}{\ddot{x}_{l0}}, \tag{32}$$

Where $\ddot{x}_l$, $\ddot{x}_{l0}$, x_i and x_0 are the peak controlled and uncontrolled accelerations and controlled and uncontrolled displacements, respectively.

$$J_6 = \frac{1}{n}\sum \frac{\ddot{x}_i}{\ddot{x}_0}, \tag{33}$$

$$J_7 = \frac{1}{n}\sum \frac{x_i}{x_0}. \tag{34}$$

Table 7 Criteria performance for structures located in near-field zone of Kobe earthquake

Name of models	J_1	J_2	J_3	J_4	J_5	J_6	J_7
M21-3-P	0.4143	0.6171	0.5950	0.4346	0.5083	0.6501	0.4678
M21-3-A	0.9249	0.7135	0.5560	0.4946	0.5667	0.4566	0.5572
M15-2-P	0.4808	0.5803	0.7422	0.6298	0.6045	0.7179	0.7777
M15-2-A	0.5728	0.6362	0.6196	0.6238	0.7727	0.7850	0.8083
M9-1-P	0.5784	0.6133	0.7534	0.6024	0.5230	0.5570	0.7797
M9-1-A	0.4339	0.6437	0.8487	0.6752	0.4379	0.6519	0.8532

Table 8 Criteria performance for structures located in far-field zone of Kobe earthquake

Name of models	J_1	J_2	J_3	J_4	J_5	J_6	J_7
M21-3-P	0.4064	0.5737	0.5479	0.5268	0.6083	0.7306	0.7838
M21-3-A	0.8657	0.7176	0.5293	0.5589	0.6904	0.5281	0.7237
M15-2-P	0.5092	0.5944	0.6716	0.5243	0.5551	0.7762	0.6407
M15-2-A	0.6134	0.6744	0.6672	0.6484	0.8003	0.8258	0.7413
M9-1-P	0.5666	0.7088	0.7355	0.5657	0.5578	0.7324	0.7122
M9-1-A	0.4430	0.6891	0.7741	0.6003	0.4556	0.7154	0.7514

Table 9 Criteria performance for structures located in near-field zone of Chi–Chi earthquake

Name of models	J_1	J_2	J_3	J_4	J_5	J_6	J_7
M21-3-P	0.3860	0.4369	0.4119	0.4609	0.6084	0.6804	0.5569
M21-3-A	0.4785	0.5456	0.4969	0.5219	0.6621	0.6568	0.6587
M15-2-P	0.5303	0.6074	0.5913	0.5176	0.5553	0.6804	0.639
M15-2-A	0.6673	0.6316	0.4882	0.5224	0.8285	0.8985	0.7364
M9-1-P	0.5554	0.7342	0.9229	0.7425	0.3280	0.7625	0.7425
M9-1-A	0.5191	0.7185	0.8823	0.7356	0.3399	0.8263	0.9636

Table 10 Criteria performance for structures located in the far-field zone of Chi–Chi earthquake

Name of models	J_1	J_2	J_3	J_4	J_5	J_6	J_7
M21-3-P	0.4098	0.4678	0.3985	0.3878	0.4417	0.7123	0.4964
M21-3-A	0.5468	0.4958	0.4041	0.4023	0.6082	0.6780	0.5221
M15-2-P	0.3877	0.4120	0.5701	0.4153	0.5196	0.6046	0.4909
M15-2-A	0.5243	0.5087	0.5562	0.5295	0.6266	0.6215	0.6238
M9-1-P	0.5554	0.5554	0.4792	0.4792	0.5568	0.5568	0.6665
M9-1-A	0.4363	0.6119	0.7061	0.5577	0.4269	0.5798	0.7009

The smaller the numerical values for these criteria, the better is the performance of the controller. According to the obtained results listed in Tables 7, 8, 9 and 10, using this control method led to control of both acceleration and displacement in the near- and far-field zones in such a way that this reduction was more in the structures in which the optimized PSO algorithm had been used rather than the ones without this algorithm. In Fig. 10, the efficiency of using the algorithm control with respect to an arbitrary one in the defined performance criteria was investigated by varying the height and earthquake frequency.

The positive values in Fig. 10 represent lower efficiency in using the optimized PSO algorithm compared with not using it. According to the results, the J_3, J_4, J_2, J_6, J_7 criteria illustrate positive effects of using algorithm control to control short buildings for both the external excitation zones. On the other hand, for the J_1 and J_5 criteria, not using the PSO algorithm in the installed actuators led to a better performance in the defined criteria. The overall results showed that the criteria of J_3, J_4, J_6, J_7, J_2 were reduced by 20, 11.11, 5, 5.9 and 5 %, on average, respectively, for all the earthquakes in the short buildings. Furthermore, except for the J_3 criterion, the other performance criteria for the structures with medium heights have better performance in the buildings with optimized actuators compared to those with unoptimized actuators. The J_1, J_2, J_4, J_5, J_6, J_7 criteria led to average reductions of 21.28, 14.66, 15.32, 21.74, 4.99 and 14.99 %, respectively, for the

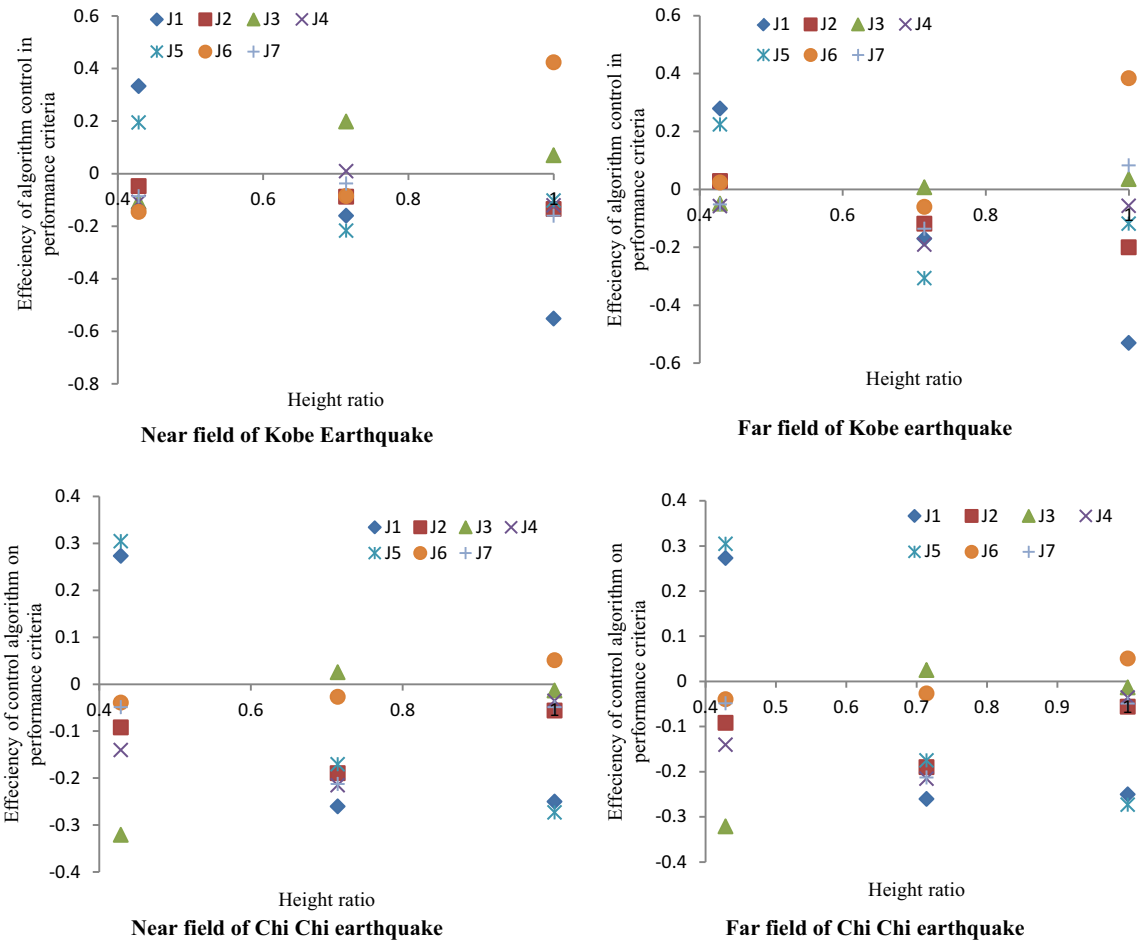

Fig. 10 Efficiency variations of defined performance criteria throughout the height ratio

structures with medium heights for both types of external excitation zones. The adopted control algorithm for the tall buildings completely depends on the type of the external excitation zone. All the introduced criteria except J_6 showed a good performance in the structure in which the control algorithm was used in comparison with the case in which no control algorithm was used. Therefore, the J_1, J_2, J_3, J_4, J_5, J_7 criteria were reduced on average by 39.59, 11.21, 1.93, 6.25, 19.23 and 4.39 %, respectively, under all applied earthquakes. By monitoring the input force to each actuator and the uncontrolled base shear, the input force for each actuator to control the buildings is determined.

According to Fig. 11, the base shear value was a function of the external excitation and the structure properties, which increased the base shear accompanied by the actuator force increase. Input actuator force was computed based on Eq. (16). Moreover, by increasing the shear force at the base level of the structure, the difference between actuator force obtained from the optimized and arbitrary cases was increased. Concerning the results obtained in Fig. 11, the required force for actuators varied in the range of 0.4–1.2 % of the total base shear.

Conclusion

In this study, by using active actuators in the braces, three different building heights were controlled under external excitations where concrete shear walls were used as secondary lateral load-resisting system in the buildings. The placement of actuators was implemented by using optimization employing the PSO algorithm method and arbitrarily for both near- and far-field earthquake zones. Concerning the results obtained, the performance of the controller using the PSO algorithm method was significantly better than the arbitrary placement of actuators in all seismic zones. By considering the effects of seismic zone, most actuators were placed on the upper third of the structure in tall buildings, while for the moderate and short buildings, most actuators were placed on the upper half of the structure. The defined performance criteria

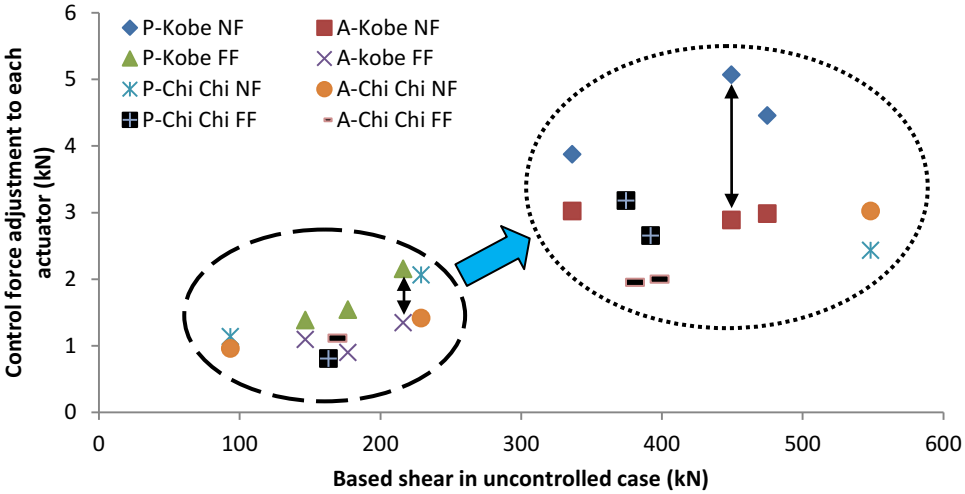

Fig. 11 The input energy to each actuator-uncontrolled base shear

demonstrated the effectiveness of the PSO algorithm controller in both seismic zones in comparison to uncontrolled and arbitrary actuator placement. Moreover, the studies showed that the actuators used consumed much less input force to control the structure and applying actuators.

References

Alavi B, Krawinkler H (2001) Effects of near-fault ground motions on frame structures. The John A. Blume Earthquake Engineering Center, Department of Civil and Environmental engineering, Stanford University, California, Report No. 138

Amini F, Vahdani R (2008) Fuzzy optimal control of uncertain dynamic characteristics in tall building subjected to seismic excitation. J Vib Control 14:1843–1867

Clerc M, Kennedy J (2002) The particle swarm-explosion, stability, and convergence in a multidimensional complex space. IEEE Trans Evol Comput 6:58–73

Federal Emergency Management Agency (2000) Prestandard and Commentary for the Seismic Rehabilitation of Buildings (FEMA 356), prepared by the SEAOC, ATC, and CUREE Joint Venture for the Federal Emergency Management Agency, Washington, DC

Galal K, Ghobarah A (2006) Effect of near-fault earthquakes on North American nuclear design spectra. J Nuclear Eng Design 236:1928–1936

Ghali A, Neville AM, Brown TG (2003) Structural analysis: a unified classical and matrix approach. Taylor and Francis, London

International Institute of Earthquake Engineering and Seismology (IIEES) (2007) Instruction for Seismic Rehabilitation of Existing Buildings (ISREB), Management and Planning Organization of Iran, Publication

Kenedy J, Eberhart R (1995) Particle swarm optimization. In: Proceeding of the IEEE International Conference on Neural Networks, Perth, Australia. 4:1942–1948

Kennedy J, Eberhart R, Shi Y (2001) Swarm intelligence. Morgan Publishers, San Francisco

Keshavarz H, Mastali M, Gerami M, Abdollahzadeh D (2011) Investigation of performance of X-braced frames in near and far fields. In: International Conference on Earthquake Engineering and Seismology, Islam Abad, Pakistan

Kheyroddin A, Abdollahzadeh D, Mastali M (2014) Improvement of open and semi-open core wall system in tall buildings by closing of the core section in the last story. Int J Adv Struct Eng 6:1–12

Kwok NM, Ha QP, Nguyen TH, Li J, Samali B (2006) A novel hysteretic model for magnetorheological fluid dampers and parameter identification using particle swarm optimization. Sens Actuators A Phys 132:441–451

Shayeghi H, Jalili A, Shayanfar HA (2008) Multi-stage fuzzy load frequency control using PSO. J Energy Convers Manag 49:2570–2580

Shayeghi A, Shayeghi H, Eimani Kalasar H (2009) Application of PSO technique for seismic control of tall building. Int J Electr Comput Eng 4:293–300

Smith BS, Coull A (1991) Tall building structures: analysis and design. Wiley, New York

Stewart JP, Chiou SJ, Bray JD, Graves RW, Somerville PG, Abrahamson NA (2001) Ground Motion Evaluation Procedures for Performance-Based Design, A report on research conducted under grant no EEC-9701568 from the National Science Foundation. University of California, Berkeley

Symans MD, Constantinou MC (1999) Semi-active control systems for seismic protection of structures: a state-of-the-art review. J Eng Struct 21:469–487

Yang JN, Agrawal AK, Samali B, Jong-Cheng Wu (2004) Benchmark problem for response control of wind-excited tall buildings. J Eng Mech 130:437–446